

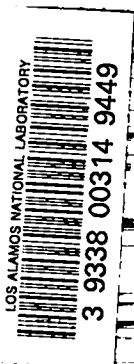
LA-3735

C.3

CIC-14 REPORT COLLECTION
REPRODUCTION
COPY

LOS ALAMOS SCIENTIFIC LABORATORY
of the
University of California
LOS ALAMOS • NEW MEXICO

A Cesium
Magnetohydrodynamic
Coaxial Arc Jet



UNITED STATES
ATOMIC ENERGY COMMISSION
CONTRACT W-7405-ENG. 36

LEGAL NOTICE

This report was prepared as an account of Government sponsored work. Neither the United States, nor the Commission, nor any person acting on behalf of the Commission:

A. Makes any warranty or representation, expressed or implied, with respect to the accuracy, completeness, or usefulness of the information contained in this report, or that the use of any information, apparatus, method, or process disclosed in this report may not infringe privately owned rights; or

B. Assumes any liabilities with respect to the use of, or for damages resulting from the use of any information, apparatus, method, or process disclosed in this report.

As used in the above, "person acting on behalf of the Commission" includes any employee or contractor of the Commission, or employee of such contractor, to the extent that such employee or contractor of the Commission, or employee of such contractor prepares, disseminates, or provides access to, any information pursuant to his employment or contract with the Commission, or his employment with such contractor.

This report expresses the opinions of the author or authors and does not necessarily reflect the opinions or views of the Los Alamos Scientific Laboratory.

Printed in the United States of America. Available from
Clearinghouse for Federal Scientific and Technical Information
National Bureau of Standards, U. S. Department of Commerce
Springfield, Virginia 22151

Price: Printed Copy \$3.00; Microfiche \$0.65

LOS ALAMOS SCIENTIFIC LABORATORY
of the
University of California
LOS ALAMOS • NEW MEXICO

Report written: January 1967

Report distributed: September 6, 1967

A Cesium
Magnetohydrodynamic
Coaxial Arc Jet

by

A. W. Blackstock
D. B. Fradkin
D. J. Roehling
T. F. Stratton





A CESIUM MAGNETOHYDRODYNAMIC COAXIAL ARC JET

by

A. W. Blackstock, D. B. Fradkin, D. J. Roehling, and T. F. Stratton

ABSTRACT

A cesium-fueled magnetohydrodynamic arc jet was operated between 4 and 12 kW at magnetic field strengths up to 1000 G. Electrostatic probe, spectroscopic, and microwave measurements were made on the exhaust beam. Beam momentum was determined from the deflection of a downstream sieve. The magnitude and position of Hall currents was determined using magnetic loop pickup coils. The overall arc voltage is a linear function of applied axial magnetic field strength. The thrust is a linear function of the product of the arc current and applied axial magnetic field strength, and is of a magnitude too great to be produced by the measured Hall currents. A partial theory is developed that describes the functional dependence of the arc voltage and thrust. Data are presented that show mass entrainment was present and that when the arc is operated with mass entrainment the exhaust velocity is predicted by the Alfvén "critical velocity."

LIST OF SYMBOLS

A	area	λ	mean free path
B	magnetic field strength	l	length
D	diffusion coefficient	ϕ	ionization potential
E	electric field strength	ρ	mass density
e	electron charge: -1.6×10^{-19} C	τ	collision time
I	current	ω	angular frequency
J	current to probe	<u>Subscripts</u>	
j	current density to probe	calor	calorimetric
k	Boltzmann constant	D	directed
L	energy of condensation, torque	e	electrons
M, m	mass	i	ions
\dot{M}, \dot{m}	mass flow rate	nom	nominal
n	number density	p	probe
P	power, angular momentum	r	radial
q	ion charge: $+1.6 \times 10^{-19}$ C	s	at the sheath edge
R, r	radius	sat	saturated
T	temperature, thrust	th	thermal
U_c, v_c	critical velocity (see Discussion)	∞	free stream condition
V	voltage		
v	velocity		
W_n	directed energy		
α	radius ratio		

INTRODUCTION

Arcs that generate a plasma by the discharge of electrical current between short coaxial electrodes in the presence of an applied, axially symmetric magnetic field are called either magnetohydrodynamic (MHD) or magnetoplasmadynamic (MPD) arcs. These plasma sources have been studied in many laboratories for space propulsion application.¹⁻⁷ The experiments described in this report are concerned with a cesium plasma generated by such a device. Macroscopic properties of the arc and the emergent beam were investigated, including the dependence of the arc current and voltage on the magnetic field, the momentum and energy flow in the beam, and the location of certain circulating currents in the arc region. The electron density and temperature and the ion streaming velocity and temperature were established from an analysis of the currents to single and double electrostatic probes.

Cesium is an unusual discharge material because its ions are unusually massive compared to the more standard propellants such as hydrogen, nitrogen, and

argon. However, it offered several advantages for our studies. The low first ionization potential permitted ready attainment of a fully ionized plasma. The low melting point allowed use of a relatively simple feed system. Because of the different ratio of the gyro frequency to the collision frequency for ions and electrons, the development of Hall currents was favored by the heavy gas plasma. Lastly, we wanted to determine if exhaust velocities corresponding to directed particle energies considerably in excess of the applied voltage could be reached with cesium, as had been reported for many lighter propellants.

APPARATUS

The arc structure was mounted vertically, as shown schematically in Fig. 1. The outer electrode was made of tantalum, 3.75-cm i.d., and was brazed into a water-cooled, copper mounting plate. The central electrode, made of tungsten, was 2.5-cm o.d. Cesium was fed to the interior of the center electrode, and the cesium emerged through 12 holes (0.12-cm diam) along 45° radii of the spherical

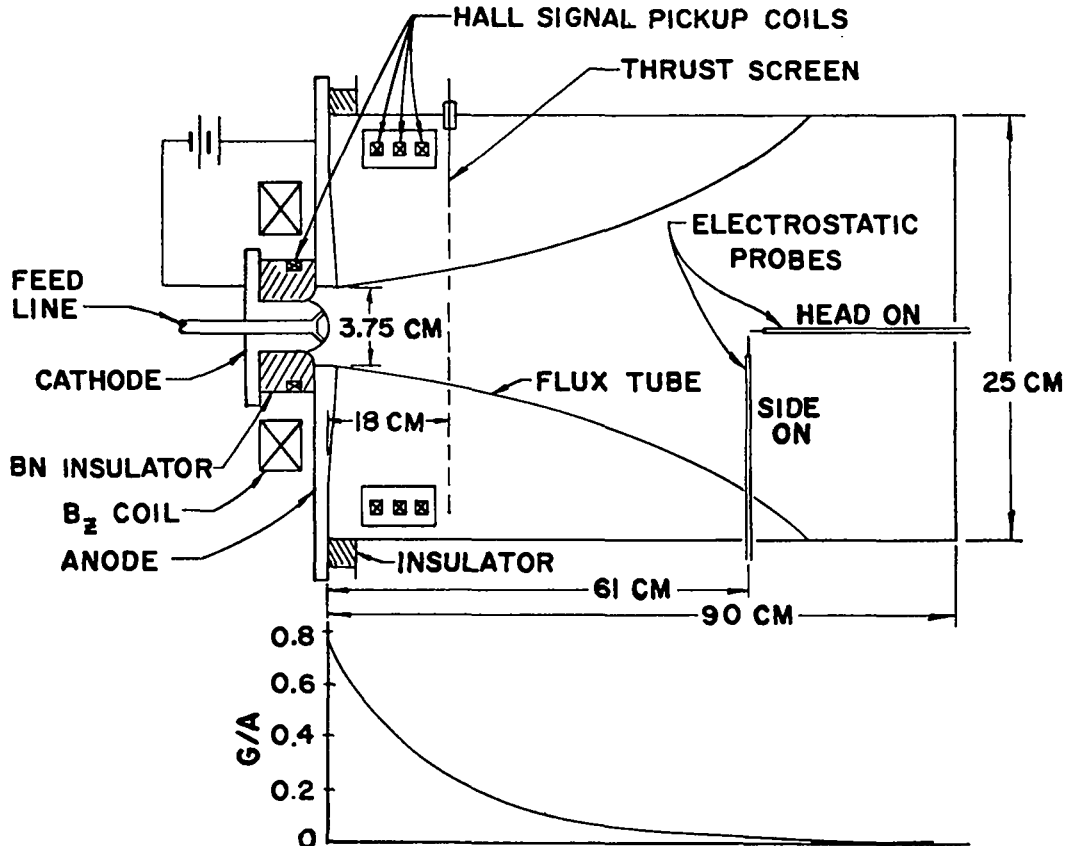


Fig. 1. Schematic of cesium arc jet showing center-line magnetic field strength.

electrode tip. The total area of the holes was 0.14 cm^2 . The insulator was machined from commercial grade boron nitride. During many months of operation, the electrodes never required replacement. The insulator was sometimes damaged by the development of radial cracks after prolonged operation at arc powers in excess of 10 kW.

The low melting temperature of cesium (30°C) allowed all parts of the arc structure and vacuum enclosure to be raised above the melting point by introducing hot water into the coolant passages. Arc startup was accomplished in vacuum by introducing cesium liquid into the center electrode chamber with voltage on the arc electrodes. Arc initiation was immediate as soon as a liquid film flowed over the exposed insulator face. If, after arc operation and shutdown, the electrodes were shorted by a residual liquid layer, arc initiation was always achieved at a short-circuit current less than 1000 amp.

Cesium was expelled from a positive-displacement bellows and piston assembly and was delivered through a heated line into the center electrode. A variable-speed dc motor drove the bellows and piston through gear reduction boxes and a screw on the bellows shaft. No difficulty was encountered with any aspect of the positive-displacement cesium feed. Calibrations of the rate of delivery of cesium as a function of motor armature voltage and gear ratio were obtained with water and a graduated pipette; the calibrations were reproducible and independent of the bellows position. Cesium that collected on the bottom plate of the experimental enclosure was returned to a reservoir after dropping through an insulating section.

The arc exhausted into a vacuum enclosure consisting of a column of water-cooled brass tubes with Teflon insulators between sections. To protect these insulators from short circuits and radiation from the arc, they were covered by protective skirts. The vacuum enclosure was 25 cm in diameter and 90 cm long. An oil diffusion pump evacuated the system through a 10-cm-diam pipe at the top of the enclosure. Base vacuums of 5×10^{-7} torr were obtained, and usual pressures of noncondensable gases during arc operation were 2×10^{-5} torr. Viewing ports were kept clear of condensing cesium by heating the windows to 90°C .

A set of coils applied an axial magnetic field to the arc geometry. The coils were 44 turns, had a 32-cm i.d., a 64-cm o.d., and were 5 cm thick. The relatively large size of the coils generated a slowly diverging field. The plane of the coil was adjustable with respect to the arc electrodes, but was generally 10 cm below the cathode tip. Currents up to 2000 A could be run through the magnet. The magnetic field strength along the centerline is shown in Fig. 1.

The arc was powered from either a motor-generator set or a rectifier unit. In either case an adjustable rheostat (0.01- to 0.05-ohm impedance) in series with the arc caused the arc current and voltage to comply with the source load line. The arc current, voltage, and parameters pertaining to electrode and beam calorimetry were recorded on synchronized strip-chart recorders.

DIAGNOSTICS

Studies of the operating characteristics of the arc were divided into methods pertaining to either the gross properties of the system or local measurements in the beam. Included in the first category were arc voltage; power in the beam and electrodes; beam momentum flow, as a function of arc current; applied magnetic field strength; and cesium mass flow. The second category included studies of the optical spectrum of the beam, microwave and electrostatic probe results for the plasma density and temperatures, and determinations of the location and magnitude of circulating plasma currents.

Arc Voltage

The arc impedance was smaller with larger current, smaller with larger mass flow rate, and larger with larger axial magnetic field strength. Arc voltage as a function of current in the axial magnetic field coils is plotted in Fig. 2 for arc currents of 400 to 900 A. Patrick and Schneiderman⁸ reported a linear variation of arc voltage with the strength of the applied magnetic field for several other working fluids, and they tabulated the results according to certain characteristic velocities related to the ionization potential of the fluids. A further discussion of the linear variation of voltage in terms of plasma rotation is given in the Discussion.

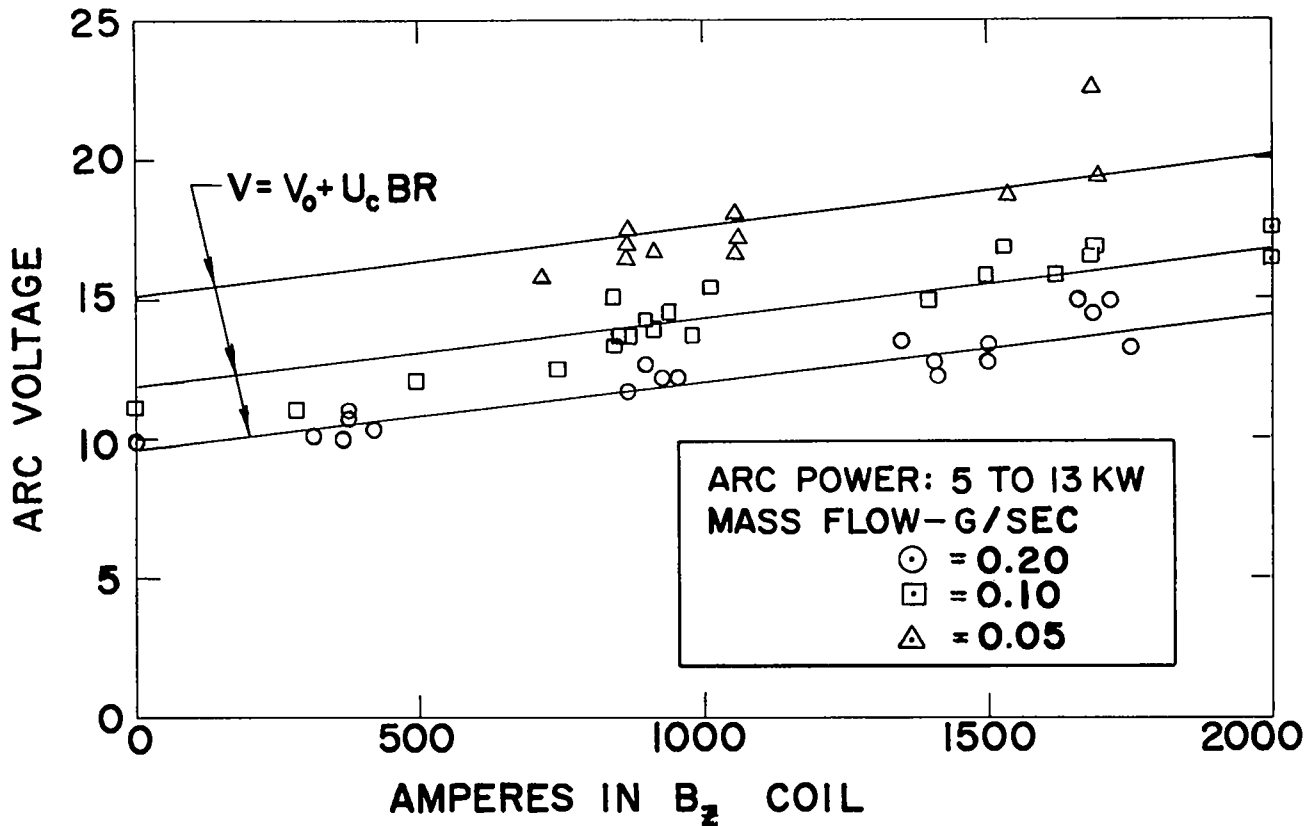


Fig. 2. Arc voltage versus magnetic field strength.

Beam Momentum Flow

There was no provision for measuring the reaction of the plasma stream on the arc and magnet structures, and the momentum flow in the beam was inferred from force measurements on plates and screens located downstream of the arc electrodes. The measurements reported here were obtained with a tungsten screen, fabricated from 0.0125-cm-diam wire, with wire spacings of 0.25 cm. The screen was large enough to intercept the entire beam and the wires ran in two directions; therefore, the geometrical fraction intercepted was 0.1. The wire size was as small as was consistent with reliable signals at the force balance. The screen could be considered in the regime of free molecular flow since the wire diameter was less than the mean free path, and the wire spacing was greater than the mean free path of the ions.

The possibility of circulating currents in the force screen was considered as a reason for the deflection of the screen. Circulating currents in the

θ direction, interacting with the radial component of the applied solenoidal field, would give rise to forces in the axial direction. The direction of the circulating currents and the direction of the radial component of the magnetic field would determine the sign of the force. A numerical estimate of the current density in the wires of the screen that would lead to the observed forces showed that the necessary current could not be supported without melting the screen; therefore, circulation of the current in the wires of the screen could not give rise to the forces observed on the screen. To prevent the circulation of part or all of the arc current directly through the screen and the supporting members the screen was electrically isolated from the arc electrodes and the vacuum enclosure. Under conditions in which the end of the vacuum enclosure was electrically connected to the anode, an arc could be established between the cathode and the end of the tank. With the screen electrically insulated from the electrodes, no force

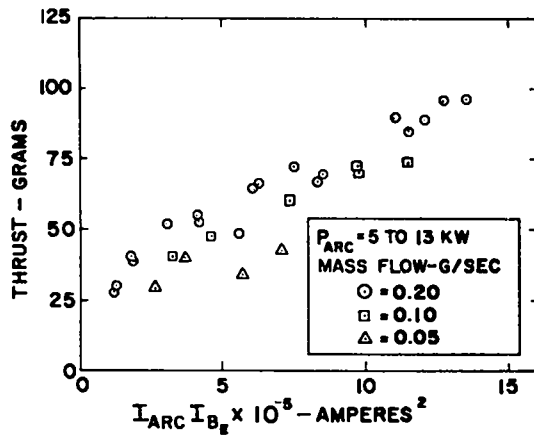


Fig. 3. Thrust versus $I_{arc} I_{Bz}$.

was registered from an arc operating in this condition.

A summary of force measurements is given in Fig. 3. The observed forces on the screen were multiplied by ten; this multiplication assumed that the screen intercepted the beam in a geometric fashion and that ions were deflected or reflected from the wires with energies that were small compared to their initial energies. Qualitatively, the force increased with both arc current and the strength of the applied axial magnetic field, and the force depended linearly on the product $I_{arc} I_{B-coils}$. A similar linear dependence of thrust on the product $I_{arc} I_{B-coils}$ was reported for other working fluids.⁹

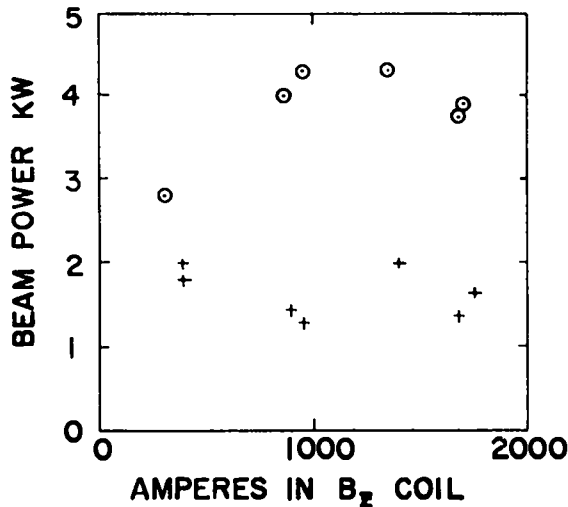


Fig. 4a. Beam power versus magnetic field strength.

○ $\dot{m} \approx 0.2$ g/sec
P \approx 10 kW

+ $\dot{m} \approx 0.2$ g/sec
P \approx 5 kW

Beam Power

The power in the beam was determined from the flow rate and temperature rise of the water cooling the walls of the vacuum enclosure. Summaries of calorimetric determinations of beam power as a function of the magnitude of the current in the field coils are shown in Fig. 4a for two conditions of arc power. Force measurements for the same runs are plotted as the ratio of the power to the force in Fig. 4b. The fraction of the input electrical power appearing in the beam was no greater than 0.4, and this fraction of the power was nearly independent of the strength of the applied magnetic field. Inasmuch as the thrust increased with the strength of the applied magnetic field, the fraction of the power in directed kinetic energy must have increased with B. However, the largest value reached by the quantity $F^2/(2\dot{m} VI)$ was 0.2.

Part of the energy carried to the beam calorimeter by ions was due to the space charge sheath between the metal of the calorimeter and the plasma of the beam. This effect has been discussed previously^{10,11} with regard to electrode losses in arcs and for electrostatic probes. The effect was similar for our electrically insulated calorimeter.

A plasma sheath affected the flux of ions and electrons to the walls. The negative sheath inhibited the flux of electrons, and hence accelerated the ions. Those electrons arriving at the wall to

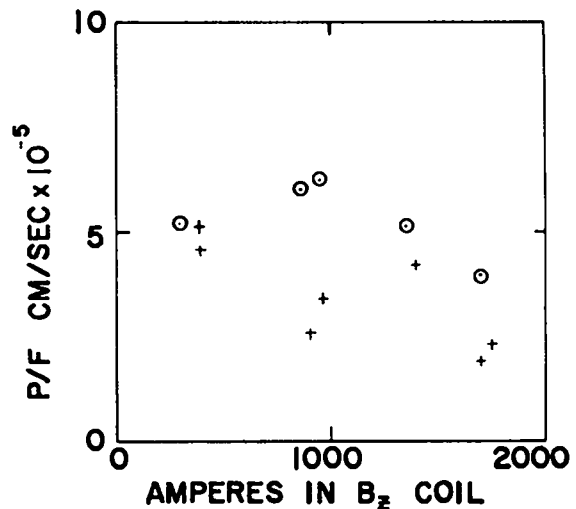


Fig. 4b. Power to thrust ratio versus magnetic field strength.

○ $\dot{m} \approx 0.2$ g/sec
P \approx 10 kW

+ $\dot{m} \approx 0.2$ g/sec
P \approx 5 kW

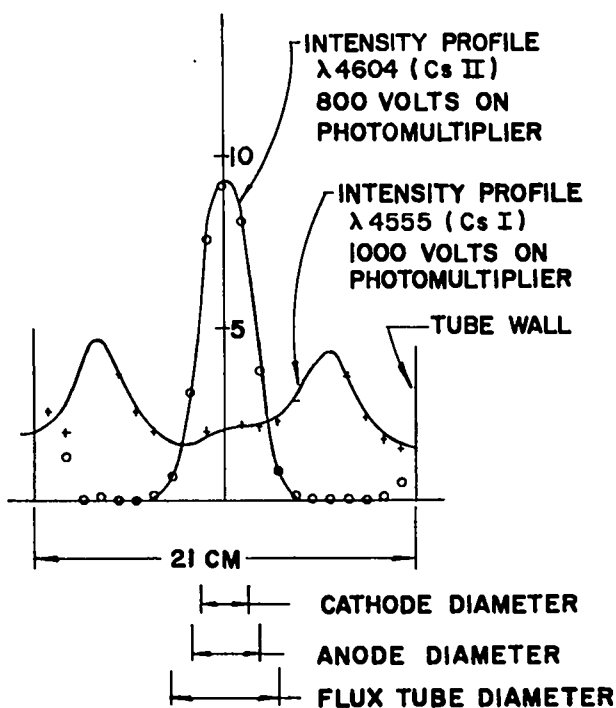


Fig. 5. Spectroscopic line strength as a function of radial position.

neutralize the ions represented the high-energy component of the electron energy distribution, and hence contributed an excess of energy to the walls. In summary, for a beam of singly charged ions, the calorimeter recorded a power

$$P_{\text{calor}} = \frac{\dot{m}e}{m_i} \left(\frac{3}{2} \frac{kT_i}{e} + 2 \frac{kT_e}{e} + V_s + \phi + W_n + L \right), \quad (1)$$

where \dot{m} is the rate of mass flow in the beam; m_i the mass of the heavy particles; kT_i and kT_e the thermal energies of the ions and the electrons, respectively; W_n the directed energy of the ions; V_s and ϕ the appropriate sheath potential and ionization potential; and L the energy of condensation. The order of magnitude of the excess energy, $(1/2 kT_e/e + V_s)$, was 2 to 5 V in our work, and represented about 0.1 to 0.25 of the total power to the calorimeter. The excess energy was supplied by thermal conduction in the electron gas between the arc and the beam stop, and hence caused a steeper gradient in the electron temperature distribution than would otherwise have occurred.

Spectra

Spectra of the plasma emerging from the arc were obtained at a point 18 cm downstream from the

cathode tip. In addition, spatial scans of the intensity of an ion and a neutral emission line were obtained by sweeping the focused image of the entrance slit of a photoelectric recording monochromator across the discharge with an oscillating mirror. The results of the scans (taken under arc conditions given in Table I) are shown in Fig. 5, where the boundaries of the anode, the cathode, and the anode projected along a magnetic field surface are indicated. The annulus of neutral emission appeared to correspond to the radius at which the electron temperature had dropped to about 0.35 eV, as determined by the relative intensity of lines in the principal series of Cs I. The absence of emission from Cs III (doubly ionized cesium) placed the electron temperature below 3 eV. The spectrum of the plume remained qualitatively unchanged for 50 cm downstream (the limit of observation). Visual observations and spectral scans showed that the beam diameter was independent of the magnetic field strength.

Electrostatic Probe Measurements

Electrostatic probes were constructed from 0.3-cm diam, sheathed Chromel-Alumel thermocouples, with 0.05-cm diam wires. The thermocouple tip was cut off, and approximately 0.1 cm of the original magnesium oxide insulation was removed. The insulation was replaced with arc-sprayed high-density alumina. The tip was then ground to provide a uniformly smooth, plane surface. For all reported data, the probes were located near the jet axis, 61 cm above the anode. The head-on probe (see Fig. 1)

TABLE I

Summary of Arc Parameters and Results Obtained for Plasma Parameters from Electrostatic Probe Measurements

Arc Parameters	Plasma Parameters
$V_{\text{arc}} = 13.4 \text{ V}$	$T_e = 1.05 \text{ eV}$
$I_{\text{arc}} = 690 \text{ A}$	$T_i = 0.51 \text{ eV}$
$I_{\text{Bz}} = 900 \text{ A}$	$J_{e\text{sat}} = 100 \text{ mA}$
Thrust = 60 g	$J_{i\text{sat}} \text{ (head on)} = 1.14 \text{ mA}$
$P_{\text{beam}} = 2.7 \text{ kW}$	$J_{i\text{sat}} \text{ (side on)} = 0.36 \text{ mA}$
$\dot{m}_{\text{nom}} = 0.1 \text{ g/sec}$	$v_D = 2.4 \times 10^5 \text{ cm/sec}$
	$n_o = 1.6 \times 10^{13} \text{ cm}^{-3}$

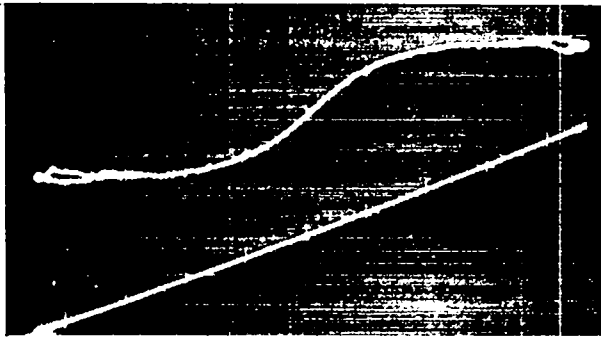


Fig. 6a. Floating symmetric double-probe trace.
Top Trace: Probe characteristic, 1 mA/division
Bottom Trace: Voltage versus voltage reference, 5 V/division

was supported from a port at the top of the vacuum vessel. The side-on probe was inserted through a gland in the side of the vacuum chamber.

Readout of the probe current and voltage was obtained on a dual-beam oscilloscope, with the probe current appearing as the voltage across fixed resistors. The probe voltage sweep was approximately ± 12 V. The probe circuit allowed shifting from floating double-probe to grounded single-probe traces for either of the two probes. Complete single-probe traces were obtained by reading the voltage across a 1-ohm resistor, and the saturated ion current portion of the trace was obtained by reading the voltage across an 11-ohm resistor. No change in amplifier gain was necessary, and the possibility of dc shifts in the amplifiers was eliminated.

After a steady arc was established, three traces were taken with each probe at each arc oper-

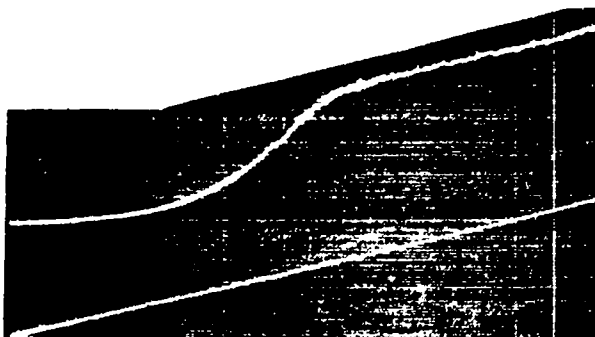


Fig. 6b. Complete single-probe trace.
Top Trace: Probe characteristic, 50 mA/division
Bottom Trace: Voltage versus voltage reference, 5 V/division

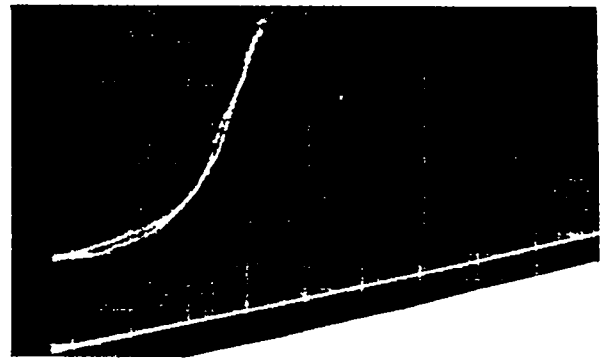


Fig. 6c. Saturated ion current portion of single-probe trace.
Top Trace: Probe characteristic, 1 mA/division
Bottom Trace: Voltage versus voltage reference, 5 V/division

ating condition. These traces were a floating double-probe characteristic, a complete single-probe characteristic, and a single-probe characteristic of the saturated ion current region. Samples of these traces are reproduced in Figs. 6a, 6b, and 6c, respectively. Fig. 7 is a semilogarithmic plot of Fig. 6b. The results for the plasma parameters, obtained in accordance with the theory developed in the Appendix, are summarized for a typical operating condition in Table I. Double-probe traces provided a check on the single-probe results when analyzed with the theory of the double electrostatic probe given by Chen.¹² From the head-on double probe,

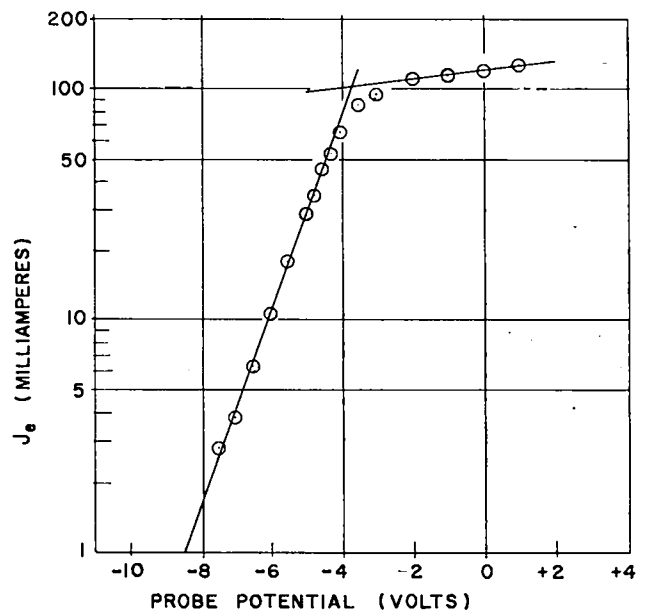


Fig. 7. Semilogarithmic plot of electrostatic probe trace.

$T_e = 1.1$ eV and $J_{i\text{ sat}} = 1.3$ mA: in good agreement with the single-probe results.

Defining the plasma potential as the voltage at the intersection of the two straight-line portions of the semilogarithmic plot of probe electron current versus v_g ,¹³ the plasma potential was -3.7 V relative to the anode potential.

Probe results obtained over a range of arc parameters (arc currents from 500 to 800 A, magnet currents from 870 to 1500 A, and mass flows of 0.1 and 0.2 g/sec) indicated little change in the values of T_e , T_i , and v_D given in Table I. The change of density with operating parameters is discussed later in this section.

The validity of the probe results was considered. The current densities to a probe in a quiescent cesium plasma, with $T_i \ll T_e$, are:

$$j_{i\text{ sat}} = 0.61 n_{\infty} q \left(\frac{kT_e}{m_i} \right)^{1/2} \quad (2a)$$

$$j_{e\text{ sat}} = \frac{n_{\infty} e}{4} \left(\frac{8kT_e}{\pi m_e} \right)^{1/2} \quad (2b)$$

At an electron temperature of 1.1 eV, in cesium, the ratio of the saturated electron current to the saturated ion current is given by Eq. (2) as 320. Theory showed that the ratio decreased with increasing ion temperature. The quiescent plasma condition was most nearly duplicated by taking the ratio of the saturated electron current from the head-on probe to the saturated ion current from the side-on probe. The resulting experimental ratio was 280.

The discussion in the Appendix assumes that the electron current to the head-on probe was unaffected by the magnetic field, and the directed velocity was computed from Eqs. (A18) and (A20). The velocity could also be inferred from the ion currents to the head-on and the side-on probes, which were unaffected by the presence of a magnetic field. The saturated ion current density to the head-on probe was nqv_D ; Eq. (2a) gives the saturated ion current density to the side-on probe. Solving for the directed velocity, $v_D = 2.2 \times 10^5$ cm/sec, showing that the probe results were self-consistent for the flow velocity of the ions.

Equation (1) describes the power deposited by a streaming plasma in an electrically insulated beam

stop. A total energy per particle ($m_i P_{\text{calor}}/m_e$) of 15.5 eV was obtained upon substitution of the appropriate plasma parameters from Table I and the excitation and sheath voltage appropriate to a singly ionized cesium gas, at an electron temperature of 1.0 eV ($v_g = 4$ V). If the total energy on the axis were representative of the entire beam, and the beam power to the calorimeter was 2.7 kW, the quantity em/m_i was 174 A. The corresponding mass flux of 0.24 g/sec of singly charged ions was in poor agreement with the nominal mass flow of 0.1 g/sec introduced from the piston, but this mass flow was in good agreement with the flow of 0.25 g/sec derived from F/v_D .

Other indications were observed of inconsistencies between the rate of mass flow introduced into the arc from the positive displacement piston and the mass flow carried by the beam. One example is illustrated in Fig. 8, where the saturated electron current to the side-on electrostatic probe is plotted against current in the applied magnetic field coils, with the mass flow rate from the piston as a parameter. There was a pronounced variation of the saturated electron current (closely related to the plasma density) as a function of

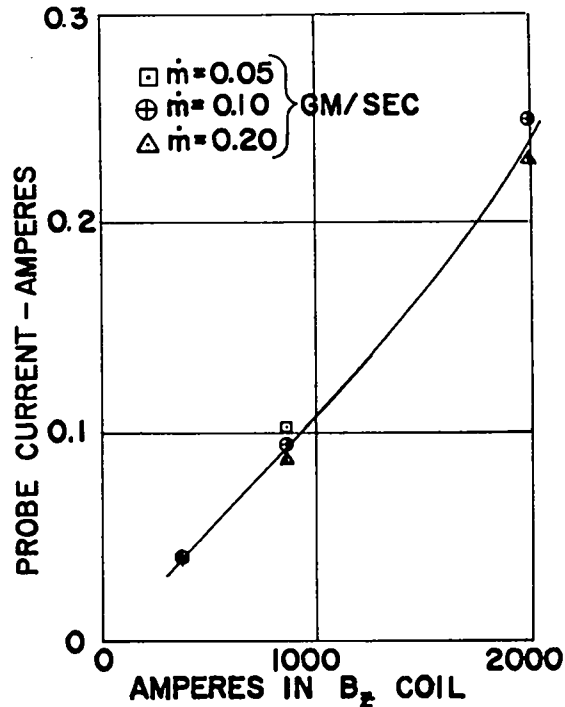


Fig. 8. Saturated probe current versus magnetic field strength as a function of mass flow.

the applied magnetic field, but there was no discernible dependence on \dot{m} . The possible influence of the magnetic field on electron current collection to electrostatic probes is discussed in the Appendix, where it is shown that the correction to the saturated electron current due to magnetic field effects was less than 12% for our experimental conditions.

In the face of these uncertainties with regard to the mass flow in the beam, the streaming velocity of the plasma could not be inferred with any reliability from the ratio of the beam momentum flow to the rate of mass introduction from the piston. The reason for the discrepancy was not understood, but it was believed that the arc was able to attach to the outside of the anode cylinder, and onto the flat surface of the anode mounting plate, where liquid cesium was available for entrainment into the discharge.

Microwave Measurements

The plasma electron density determinations from the electrostatic probes were supported by measurements of the transmission of 35-GHz microwaves through the arc plasma. The transmission measurements indicated whether the plasma density was greater than or less than the cutoff, or critical, plasma electron density. For a test frequency of 35-GHz, the cutoff electron density was $1.52 \times 10^{13} \text{ cm}^{-3}$. The dominant TE_{10} mode was propagated in the rectangular wave guide, with the electric field parallel to the short side of the wave guide. The magnetic field had a longitudinal component and a component parallel to the long side of the wave guide. The microwave horns were oriented so that the electric field of the incident wave was parallel to the applied magnetic field of the plasma jet.

No increase in the reflected signal due to the plasma was observed in any of the microwave measurements. The microwave beam was introduced into the vacuum enclosure through Pyrex windows. The minimum reflected signal with no arc was about 0.1 of the transmitted signal, even though the thickness of the glass was very close to an odd multiple of $\lambda/2$ (Ref. 14), and the reflected signal was minimized with an impedance matching transformer. An experiment in which the plasma was simulated by a

copper cylinder substantiated the supposition that the signal reflected from the plasma was small compared to the fixed reflections.

A comparison of electrostatic probe and microwave density measurements is given in Table II.

Table II

Electrostatic Probe and Microwave Density Measurements	
<u>Electrostatic Probe Density (cm^{-3})</u>	<u>Microwave Transmission</u>
4.3×10^{13}	Cutoff
2.2×10^{13}	Cutoff
1.6×10^{13}	Transmission

The smallest electron density from electrostatic-probe measurements for which microwave cutoff was obtained was $2.2 \times 10^{13} \text{ cm}^{-3}$, or 1.5 times the cutoff density. A recent comparison¹⁵ of plasma electron density measurements by electrostatic probes and microwaves gave agreement within a factor of 2 to 10, at distances from the source which were comparable to the measurements reported here.

Plasma Current Distribution

Experimental measurements of the momentum flow carried by the emergent plasma showed good correlation between momentum flow and the product $I_{\text{arc}} I_{\text{B-coils}}$ (see Fig. 3), where I_{arc} is the arc current and $I_{\text{B-coils}}$ is the current carried by the coils producing the axial magnetic field. A dependence of this sort suggested that a portion of the momentum transferred to the plasma arose through the interaction of a ring of current in the plasma (I_{θ}) with the current in the axial field coils. The existence of such a plasma current could be verified by probing the steady-state magnetic field distributions internal and adjacent to the plasma column, or, more simply, by detecting the change in magnetic flux through a magnetic loop around the plasma column when the arc was extinguished. The second procedure could not yield detailed information about the distribution of current and current density, but it would allow the measurements to be made outside the region of high arc power density without disturbing the plasma. The qualitative features of a ring current, such as mean radial and axial position, and magnitude of circulating current, could be

established by determining the flux linkage at several axial and radial locations.

Coils consisting of 200 turns of 0.02-cm diam insulated wire were positioned at the radial and axial locations shown in Fig. 1. Signals induced in these coils upon arc extinction were integrated by passive RC integrator networks of 0.25-sec time constant and were displayed on oscilloscopes. The integrated signal level varied between a fraction of a millivolt and 2 mV. The long RC integration time was necessary because of the slow rate of fall of the arc current (approximately 10 msec) and the long times required for penetration of the axial magnetic fields through the heavy walls and flanges of the vacuum enclosure (measured to be 30 msec). The coils adjacent to the beam were encased in a stainless steel shell and were cooled with Dow Corning Corp. 200 fluid at 200 psi. The time constant of the shell was 0.3 msec; this constant was small compared to the other relevant time constants. The possibility of a discrepancy between the ac and dc coupling coefficients was tested by comparing the loop signals generated by a single-turn coil, powered and switched by the arc power supply, with the signals calculated under dc coupling conditions, as a function of the axial location of the single-turn loop. There were appreciable discrepancies between the measured and calculated coupling coefficients for all four pickup loops, and it was therefore necessary to use the experimentally determined coefficients to obtain the positions and magnitudes of the circulating currents.

Qualitative features derived from the sign and relative magnitudes of the signals induced in the loops are:

- 1) The sign of the signal induced in the B_z coils corresponded to an electron drift in the direction $\vec{E}_r \times \vec{B}_z$ (current in the direction $-\vec{E}_r \times \vec{B}_z$).
- 2) Reversing the sign of \vec{B} reversed the signal, but had no other effect.
- 3) Reversing the sign of \vec{E} reversed the signal and had the following auxiliary effects. When the electric field was radially inward (center electrode negative), the circulating current was located exterior to the arc electrode region, the magnitude of the current was the order of, or somewhat smaller than, the arc current, and an emergent, fully ionized stream of plasma was obtained, which carried

approximately one-third of the input electrical power to the arc. When the electric field was radially outward (center electrode positive), the sign of the loop signal was reversed and reduced in amplitude by approximately an order of magnitude. In addition, there was no visible emergent plasma stream, and the input electrical power was almost completely recovered in the arc electrodes.

If these qualitative features were associated with a Hall current, some insight into the mechanisms at work may be obtained by referring to Fig. 9. The sense of the drift giving rise to the Hall current is indicated in the direction $\vec{E} \times \vec{B}$ (specifically the θ component $E_r B_z$). The interaction of the Hall current associated with a differential drift between electrons and ions and the applied magnetic field produced a body force $\vec{J}_\theta \times \vec{B}$, which had components both radially and axially. Reversing the direction of the applied magnetic field reversed both \vec{J}_θ and \vec{B} ; it did not reverse the direction of the cross product. Reversing the electric field, however, reversed the direction of \vec{J}_θ without affecting \vec{B} , so that the body force due to $\vec{J}_\theta \times \vec{B}$ reversed sign. It should be noted, again referring to Fig. 9, that with the polarity of the applied voltage such as to establish an electric field inwards, the $\vec{J}_\theta \times \vec{B}$ forces were directed inwards and away from the plane of the coil producing the applied magnetic field. Reversal of the electric field (center electrode positive) caused the forces to be outward and toward the plane of the magnet coil. Hence, there was an explanation for both the qualitative difference in arc behavior with reversal of the electric field and for the simple

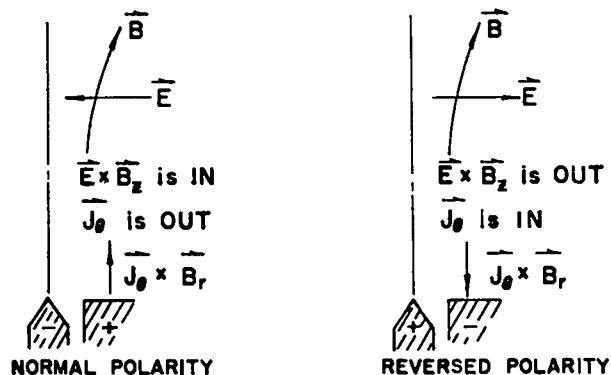


Fig. 9. Effect of arc polarity reversal.

change in the sign of j_θ with reversal of the direction of the applied magnetic field.

Qualitative features of the relative amplitudes of the signals in the three downstream loops allowed general statements to be made about the magnitude and location of the circulating plasma currents. First, at currents through the magnet coils above 500 A, the relative amplitudes of the signals in the downstream coils were equal, within 20%, and were about 3.0 ± 0.3 times greater than the signal in the coil in the insulator. This means that the circulating current was distributed in a reasonably uniform fashion over a length at least 12 cm downstream of the cathode tip. With smaller currents in the B_z coil (less than 150 A), the coils closer in received the greater signals, until, at 100 A in the B_z coil, the ratio of the signals in the closest to the farthest coil was about 1.5. This would occur if the current were located no farther than 7 cm downstream of the cathode tip.

A qualitative examination of the probe signals corresponding to an arc current of 620 A and 660 A in the B_z coils showed that the circulating currents were located downstream of the arc electrodes and that a reasonable fit of the relative amplitudes of the downstream loop signals and the insulator coil signal was obtained if the θ currents were distributed uniformly between 5.5 and 9.5 cm downstream of the cathode, at a mean radius of 1.7 cm., and having a magnitude of 37.5 A per centimeter of length for a total Hall current of 150 A. The relative magnitudes of j_r and j_θ were estimated by assuming that the region of radial current density corresponded to the region of ring currents and the radial extent of the ring currents was approximately 1 cm. For the case studied, at the mean Hall current radius of 1.7 cm, $j_\theta/j_r \approx 2.5$.

The measured dependence of the magnitude of the signals induced in the insulator magnetic pickup coils, as a function of the strength of the applied axial magnetic field, with arc current as parameter, is shown in Fig. 10. We were not able to develop a model that would produce the qualitative behavior shown by the data. The dependence of Hall currents on the strength of the applied magnetic field, as discussed by Brockman *et al.*¹⁶ and Henry¹⁷ did not agree with the shape of the experimental curves for large B_z , and it was necessary to consider effects

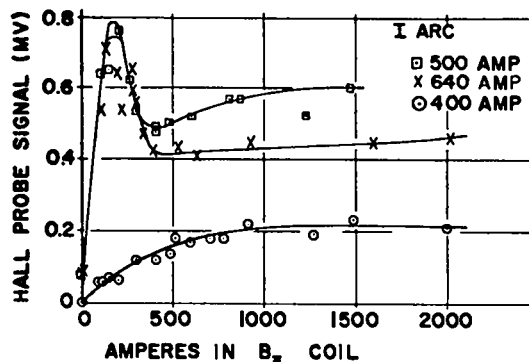


Fig. 10. Hall probe signal strength versus magnetic field strength.

other than the cancellation of the electron Hall current with an ion current that increased with the ion Hall parameter $\omega\tau_1$.

DISCUSSION

The experiments reported here do not unambiguously identify the properties of the cesium coaxial arc that produced the emergent beam. They do point to the existence of some physical processes that have been suspected but have not been specifically identified with arc operation. Some of these processes are:

1) The arc tends to be particular about the mass flow through it. The design of the arc structure allowed material to be entrained into the arc region; evidence for this is the small dependence of thrust and arc impedance characteristics on the rate of mass introduction into the arc and the independence of the plasma density inferred from electrostatic probes on mass flow.

2) For arcs operating with mass entrainment, the plasma streaming seems to be limited to the critical velocity of Alfvén,¹⁸ given by $v_{ci} = (2e\phi_1/m_1)^{1/2}$, where ϕ_1 is the ionization potential of the propellant. Heavy particle velocities much in excess of the critical velocity corresponding to the first ionization potential of cesium (2.35×10^5 cm/sec) were not observed. The linear dependence of arc voltage on B_z , characteristic of this type of arc, is interpreted as also supporting the velocity limiting effect.⁸ Recent experiments using lithium indicate that the critical velocity can be exceeded only if mass entrainment is limited.¹⁹

3) The cesium arc experiments show a linear dependence of thrust with the product $I_{arc} I_{B_z}$. The

linear dependence on arc current has been reported.^{9,20}

4) The existence of circulating currents in a direction normal to both the applied electric and magnetic fields is established for the cesium experiments. The sense of the applied electric field influences the properties of the arc and the emergent beam, presumably because of the interaction of the circulating currents with the applied magnetic field. When the circulating currents are in such a direction as to experience a repulsive force from the magnet coils, a beam is produced, and the location of the circulating currents is downstream of the arc electrodes.

Several mechanisms are available for the generation of circulating currents in the θ direction. Two mechanisms are by nature Hall currents that circulate in the direction of $-\vec{E} \times \vec{B}$. Two others are associated with the confinement of the plasma stream by the applied magnetic field. These currents are identified as follows:

1) Ions and electrons show different ratios of the gyro frequency to an averaged momentum transfer collision frequency with stationary neutrals, and as a result the electrons approach the drift velocity associated with the crossed electric and magnetic fields more nearly than do the ions.

2) Regions in which ionization occurs, either because of a transient discharge or a steady streaming of neutral gas into the discharge, support circulating currents because the inertia of the ions prevents them from accelerating to the drift velocity as quickly as the electrons.

3) Ordinary diamagnetic currents are present, reducing the magnetic field intensity interior to the plasma and allowing the applied magnetic field to support the plasma pressure.

4) Currents are present that balance the centrifugal forces in a rotating plasma confined by a magnetic field.²¹

Although the diamagnetic and centrifugal currents would exist for any heated, rotating, plasma confined to a magnetic flux tube, the Hall currents require an applied electric field in order to persist. However, the effects associated with the creation of the heated and rotating plasma, through the application of an electric field, are intimately connected to the sign of the applied voltage,

and we are not able to resolve the observed circulating current into its various components.

The pronounced dependence of the beam on the existence of the circulating currents (henceforth termed Hall currents) and the straightforward manner in which such a current interacting with the radial component of the applied magnetic field produces a force in the axial direction suggest that the linear dependence of the thrust on the applied magnetic field is due to the $j_{\theta} B_r$ force integrated over the plasma volume. Quantitatively, it appears that this is not the case.

Consider the conditions described in the section entitled Plasma Current Distribution. The magnet current was 660 A, and the Hall current was 150 A. A calculation of the reaction between the Hall currents and the magnet coils shows that the force due to the interaction $j_{\theta} B_r$ is 3.3 g. The total thrust produced at these operating conditions is 54 ± 5 g, of which 24 g is the contribution due to the magnetic interactions. Hence, the force due to $j_{\theta} B_r$ is only 15% of the magnetic force. In fact, 3.3 g is somewhat less than the magnetic force due to the interaction of the arc current and the self-field ($j_r B_{\theta}$).

If the Hall-current terms and the self-field forces are not adequate to explain the thrust produced by the external field arc, what are the alternatives? Thrust is produced by the expansion of a heated gas through a nozzle formed by the diverging magnetic field lines.²² An approximation to the thrust produced by expansion is obtained by considering the ions decoupled from the electrons, and inquiring as to the requisite ion temperature to give the measured thrust, assuming an ideal infinite expansion. Hence, $5/2 \dot{m} kT_i = 1/2 \dot{m} m_i v^2$, and, with $\dot{m} v = F$ (the thrust), the ion temperature at the source becomes $kT_i = m_i F^2/5 \dot{m}^2$. (Alternatively $kT_i = 2/5 (1/2 m_i v^2)$; i.e., the ion temperature at the source is equivalent to 0.4 of the directed energy in the beam.) It is not possible to dismiss the possibility of thrust production through thermal expansion, because, for our conditions of operation, at a thrust of 54 g and $\dot{m} = 0.2$ g/sec, the requisite ion temperature is about 23,000°K, in close agreement with the observed electron temperature. The principal objection to a thermal-expansion hypothesis is contained in the dependence of

thrust on the strength of the magnetic field. One would expect a saturation of thrust with increasing magnetic field, as the expansion becomes ideal. These experiments show a linear dependence of thrust with applied magnetic field strength and no apparent change in beam diameter with field strength.

Another possibility for the production of thrust is through the conversion of rotational energy produced by $j_r B_z$ and $j_z B_r$ interactions into beam kinetic energy. Such mechanisms have been mentioned by Ellis²³ and Hess,²⁴ but they didn't discuss in detail the consequences of a model based on rotational energy.

Consider a rotating plasma which expands through a magnetic nozzle. Two regions are defined. In the interaction region both radial and circulating currents exist and the plasma is accelerated through $j \times B$ interactions. In the nozzle region no radial currents exist. The fluid angular momentum at the beginning of the nozzle region is

$$P_\theta = \ell \rho \int_0^R r v(r) 2\pi r dr, \quad (3)$$

where, for simplicity, the plasma is assumed to have uniform density and the integral is from the axis to some radius R. Assume next that $v(r) = v_\theta$, i.e., there exists a uniform rotational velocity; then the angular momentum becomes $2/3 \pi \ell \rho v_\theta R^3$. The corresponding rotational energy is

$$W_\theta = \ell \rho \int_0^R \frac{1}{2} v^2(r) 2\pi r dr, \quad (4)$$

and for the same assumptions as before, the energy is $\pi/2 \ell \rho v_\theta^2 R^2$. The total mass in rotation is $\pi R^2 \rho \ell$. Substituting in Eqs. (3) and (4), the angular momentum becomes $2/3 M v_\theta R$, and the energy in rotation becomes $1/2 M v_\theta^2$. As this rotating mass expands, the angular momentum is conserved, and the rotational velocity at a new expanded radius is $v_{\theta_2} = v_{\theta_1} (R_1/R_2) = v_{\theta_1}/\alpha$. The energy converted to translation is $W = M/2 (v_{\theta_1}^2 - v_{\theta_2}^2) = M/2 v_{\theta_1}^2 (1 - 1/\alpha^2)$. The axial velocity from expansion is then $v = v_{\theta_1} (1 - 1/\alpha^2)^{1/2}$.

In the interaction region the torque exerted by the $j_r B_z$ force is

$$L = \iiint j_r B_z r dV. \quad (5)$$

By letting the magnetic field be constant over the

volume of integration and putting the radial current density equal to $I/2\pi r \ell$, Eq. (5) becomes $L = 1/2 B I R^2$. Now, the torque is equal to the time rate of change of angular momentum, so that $L = d/dt (2/3 M v_\theta R) = 2/3 R \dot{M} v_\theta$, in steady state. Hence, we have that

$$F = \dot{M} v = \frac{3}{4} B I R (1 - \frac{1}{\alpha^2})^{1/2}, \quad (6)$$

where B is the magnetic field strength in the interaction region. The constant coefficient multiplying the factor BIR is not very sensitive to the radial dependence of $v(r)$. For example, if the rotation is assumed to occur as a solid object, i.e. $v(r) = \omega r$, the constant becomes $\sqrt{2}/2$ instead of $3/4$.

Equation (6) represents the thrust due to electromagnetic interactions. The total thrust is given by the expression

$$F = F_{\text{aero}} + F_{\text{self}} + F_{\text{Hall}} + \frac{3}{4} B I R,$$

where F_{self} is the thrust due to self-field interactions, F_{Hall} is the thrust due to the Hall-current magnet interaction, and F_{aero} is the aerodynamic thrust, which may be a function of the propellant chosen and the input mass flow. It was shown previously that for the present operating conditions F_{self} and F_{Hall} will be quite small. Therefore,

$$F \approx F_{\text{aero}} + \frac{3}{4} B I R. \quad (7)$$

Equation (6), with $(1 - 1/\alpha^2)^{1/2} = 0.8$, which corresponds to the appropriate area ratio between the anode and the thrust screen for the magnetic-flux tube filled by the plasma beam, is plotted in Fig. 11. The data in this figure were obtained

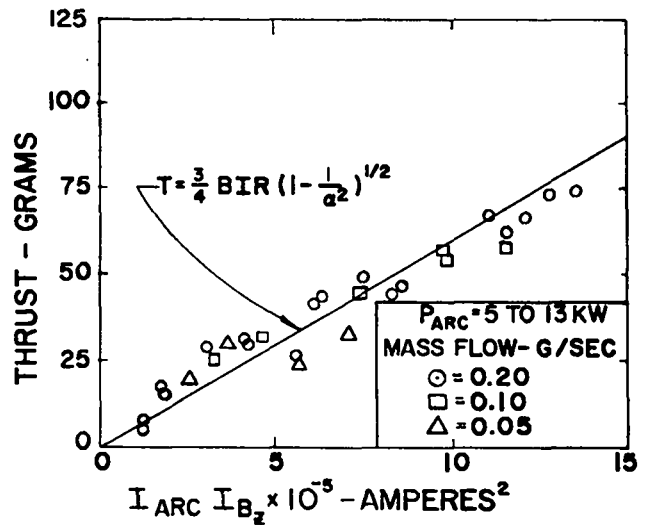


Fig. 11. Electromagnetic thrust versus $I_{\text{arc}} I_{B_z}$.

from Fig. 3 by independently fitting Eq. (7) through the data points for each of the three flow rates. Thus, F_{aero} for each flow rate was determined. The points on Fig. 11 are thus the total measured thrust less the appropriate F_{aero} . Similar quantitative agreement is found when Eq. (6) is compared with results of Bennett *et al.*⁹

A rotation of the plasma introduces a contribution to the arc voltage through the back emf, $V_r = \int_0^R E dr$. Assuming that the rotational velocity is converted to the exhaust velocity, so that $v_\theta = v_{exhaust}$, and taking an additive constant for the sheath and ohmic voltages,

$$V = V_0 + v_{exhaust} B_z R. \quad (8)$$

Patrick and Schneiderman⁸ have proposed such a dependence of arc voltage on B_z and have further assumed that the exhaust velocity is related to the limiting critical velocity of Alfvén,¹⁸ for input mass flows greater than $F/v_{critical}$. Equation (8), with $v_{critical}$ substituted for the $v_{exhaust}$, is compared to the experimental data in Fig. 2.

Both mechanisms that we have discussed as possible mechanisms for the production of axial momentum flow in external field coaxial arcs appear to have been discounted by other authors in favor of thrust production through the interaction of the Hall currents with the radial component of the applied magnetic field. For our geometry and conditions, we have shown that the Hall-current interaction is nearly an order of magnitude too small to account for the thrust. We feel that these measurements support a rotational mechanism, although there is still room for a more definitive experiment, for example, a simultaneous measurement of the axial momentum flow and the angular momentum in the beam. A rotational acceleration process should give the result that the ratio of the derivatives of the torque and the thrust taken with respect to the strength of the applied field, should be $2R/3(1 - \alpha^2)^{1/2}$.

ACKNOWLEDGMENTS

We acknowledge the helpful discussions with and encouragement from G. M. Grover. Fabrication and maintenance of the equipment was implemented by the services of R. E. Welch and R. A. Wicklin. The microwave equipment was kindly lent to us by H. Dreicer.

APPENDIX

Probe Operation in a Streaming Plasma

Consider a plane probe directed head-on into a flowing plasma. A negatively biased probe creates the potential distribution shown in Fig. A-1a, where the plasma potential is taken equal to zero. It is assumed that the flow is collisionless, and that quasineutrality holds throughout the transition region. Poisson's equation gives

$$\nabla^2 V = 4\pi e (n_i - n_e) = -4\pi (qn_i + en_e). \quad (A1)$$

The Boltzmann relation is assumed to be valid for the electrons:

$$n_e = n_{es} e^{-e(v-V_s)/kT_e}. \quad (A2)$$

The energy of singly-charged ions at the sheath consists of the thermal energy, the beam kinetic energy, and the energy acquired in falling through the negative potential V_s . The ion velocity at the sheath edge is then

$$v_{is} = \left(\bar{v}^2 - \frac{2qV_s}{m_i} \right)^{1/2}, \quad (A3)$$

where \bar{v} is the ion velocity directed along the normal to the probe due to the thermal and streaming motion.

When the probe is a perfect sink for ions²⁵ and the sheath is so thin that the area of the sheath

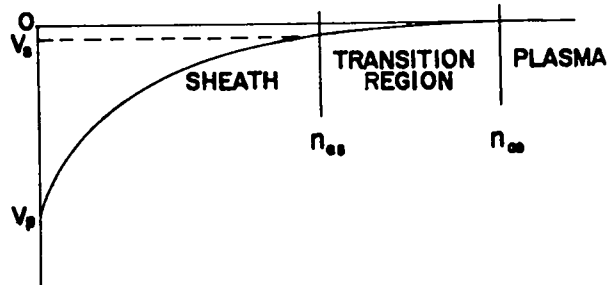


Fig. A-1a. Normal probe potential distribution.

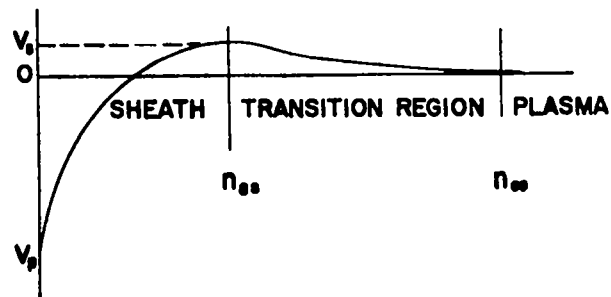


Fig. A-1b. Probe potential distribution for ion energy greater than half the electron temperature.

is approximately equal to the area of the probe, the ion current density through the sheath is a constant. Then, in the sheath region

$$j_i = qn_i \left(\bar{v}^2 - \frac{2qV}{m_i} \right)^{1/2} \quad (A4)$$

$$= q n_{is} \left(\bar{v}^2 - \frac{2qV_s}{m_i} \right)^{1/2}$$

or

$$n_i = n_{is} \left[\frac{\left(\bar{v}^2 - \frac{2qV_s}{m_i} \right)}{\left(\bar{v}^2 - \frac{2qV}{m_i} \right)} \right]^{1/2} \quad (A5)$$

Substituting Eqs. (A2) and (A5) into (A1) and integrating:

$$\frac{1}{8\pi} \left(\frac{\partial V}{\partial X} \right)^2 = n_{is} m_i \left\{ \left[\left(\bar{v}^2 - \frac{2qV_s}{m_i} \right) \left(\bar{v}^2 - \frac{2qV}{m_i} \right) \right]^{1/2} \right. \\ \left. + n_{es} kT_e e^{-e(V-V_s)/kT_e} \right\} + C \quad (A6)$$

The potential changes slowly through the transition region. At the transition region, sheath region boundary the potential begins to change rapidly. An approximate boundary condition is that $(\partial V/\partial X)^2 \approx 0$ and $V = V_s$ at $X = s$. The arbitrary constant of integration is determined with this boundary condition, and Eq. (A6) becomes

$$\frac{1}{8\pi} \left(\frac{\partial V}{\partial X} \right)^2 = n_{is} m_i \left\{ \left(\bar{v}^2 - \frac{2qV_s}{m_i} \right)^{1/2} \right. \\ \left. \left[\left(\bar{v}^2 - \frac{2qV}{m_i} \right)^{1/2} - \left(\bar{v}^2 - \frac{2qV_s}{m_i} \right)^{1/2} \right] \right. \\ \left. + n_{es} kT_e \left(e^{-e(V-V_s)/kT_e} - 1 \right) \right\} \quad (A7)$$

Since we are interested in the solution near $V = V_s$, we expand in $\Delta V = V - V_s$, and we further assume that all ions are singly charged, setting $n_{is} = n_{es}$ and $e = -q$. Then,

$$\frac{1}{4\pi n_e e^2} \left(\frac{\partial V}{\partial X} \right)^2 = \left[\frac{1}{kT_e} - \frac{1}{m_i \left(\bar{v}^2 + \frac{2eV_s}{m_i} \right)} \right] (\Delta V)^2 \quad (A8)$$

Again, at the sheath boundary, $(\partial V/\partial X)^2 \approx 0$. Hence

$$\frac{1}{kT_e} - \frac{1}{m_i \left(\bar{v}^2 + \frac{2eV_s}{m_i} \right)} \approx 0$$

and

$$V_s \approx \frac{1}{2e} (kT_e - m_i \bar{v}^2) \quad (A9)$$

Defining the nondimensional quantities $\chi_s = eV_s/kT_e$ and $\beta = m_i \bar{v}^2/kT_e$, the nondimensional sheath potential becomes

$$\chi_s = (1-\beta)/2 \quad (A10)$$

The ion current density at the sheath boundary is given by Eq. (A4). Throughout the transition region the ion and electron densities are approximately equal, so that upon substitution of Eqs. (A9) and (A2), the ion current density becomes

$$j_i = n_{\infty} q \left(\frac{kT_e}{m_i} \right)^{1/2} e^{-\chi_s} \quad (A11)$$

The case of zero ion thermal and streaming velocity gives $V_s \approx kT_e/2e$, which is the Bohm sheath criterion.²⁵ Also $\chi_s = 1/2$, so that

$$j_i = 0.61 n_{\infty} q \left(\frac{kT_e}{m_i} \right)^{1/2} \quad (A12)$$

the result obtained by Allen *et al.*²⁶

In the present formalism V_s becomes positive when the thermal and streaming energy of the ions exceeds $kT_e/2$. Equation (A6) is still valid, since electrons are repelled throughout the sheath region, and the boundary condition $(\partial V/\partial X)^2 \approx 0$ becomes exact. The corresponding potential distribution is shown in Fig. A-1b. It is physically unnecessary for the transition region first to decelerate and then accelerate ions, since current continuity may be maintained without a transition region and the sheath solution exactly matches the plasma volume. We conclude, therefore, that V_s and χ_s are zero when the thermal, or streaming energy of ions is greater than $kT_e/2$. In this case the ion current density is given by

$$j_i = n_{\infty} q \bar{v} \quad (A13)$$

Summarizing the results for ion collection:

$$\text{If } \beta < 1, \chi_s = \frac{(1-\beta)}{2} \text{ and } j_i = n_{\infty} q \left(\frac{kT_e}{m_i} \right)^{1/2} e^{-\chi_s}; \\ \text{if } \beta \geq 1, \chi_s = 0 \text{ and } j_i = n_{\infty} q \bar{v}.$$

β behaves like the Mach number. For "subsonic" flow ($\beta < 1$), a disturbance, the transition region, extends upstream from the probe. For "supersonic" flow ($\beta \geq 1$), no transition region exists, there is no upstream disturbance, and the probe simply collects the flux of ions crossing the sheath surface.

Consider now a positively biased probe. Under arc jet conditions it is reasonable to suppose that

the thermal velocity of the electrons is much greater than their directed velocity. The electron current is then due to the thermal drift.

$$j_e = \frac{1}{4} n_{\infty} e \left(\frac{8kT_e}{\pi m_e} \right)^{1/2} e^{-eV/kT_e} \quad (A14)$$

Differentiation of Eq. (A14) gives the usual expression for electron temperature, viz.:

$$\frac{kT_e}{e} = \frac{dV}{d(\ln j_e)}$$

or

$$T_e = 11,600 \frac{\Delta V}{\ln \left(\frac{j_{e2}}{j_{e1}} \right)} \text{ } ^\circ\text{K} \quad (A15)$$

A probe at the plasma potential collects a current

$$j_e \Big|_{V=0} = \frac{1}{4} n_{\infty} e \left(\frac{8kT_e}{\pi m_e} \right)^{1/2} \quad (A16)$$

so that the plasma density is given as

$$n_{\infty} = \frac{4j_e \Big|_{V=0}}{e} \left(\frac{\pi m_e}{8kT_e} \right)^{1/2} \quad (A17)$$

An arc jet exhaust will almost always be "supersonic" ($\beta \geq 1$). The effective velocity is found by taking the ratio of Eqs. (A13) and (A16):

$$\bar{v} = \frac{j_i}{4j_e \Big|_{V=0}} \left(\frac{8kT_e}{\pi m_e} \right)^{1/2} \quad (A18)$$

Consider a probe placed at right angles to the flow. The ion collection is due only to the thermal drift, so that Eq. (A11) is the appropriate expression for the ion current.

$$j_i = n_{\infty} q \left(\frac{kT_e}{m_i} \right)^{1/2} e^{-m_i \bar{v}^2 / 2kT_e} \quad (A19)$$

For this probe, $\bar{v}^2 = v_{th}^2$. Solving for v_{th}^2 ,

$$v_{th}^2 = \frac{2kT_e}{m_i} \left\{ \frac{1}{2} + \ln \left[\frac{j_i}{n_{\infty} q} \left(\frac{m_i}{kT_e} \right)^{1/2} \right] \right\} \quad (A20)$$

The directed velocity is determined, since $v_D = (\bar{v}^2 - v_{th}^2)^{1/2}$. In most cases for the head-on probe $\bar{v}^2 \gg v_{th}^2$, so that a good approximation to the drift velocity is

$$v_D = \frac{j_i}{4j_e \Big|_{V=0}} \left(\frac{8kT_e}{\pi m_e} \right)^{1/2} \quad (A21)$$

The ion temperature may be derived from Eq. (A20) by setting $kT_i = m_i v_{th}^2$.

The velocity of subsonic ($\beta < 1$) flows is found from Eqs. (A11) and (A14).

$$\bar{v}^2 = \frac{2kT_e}{m_i} \left\{ \frac{1}{2} + \ln \left[\frac{4j_e}{j_i} \left(\frac{\pi m_e}{8m_i} \right)^{1/2} \right] \right\} \quad (A22)$$

With v_{th}^2 again determined from a side probe, $v_D = (\bar{v}^2 - v_{th}^2)^{1/2}$.

Discussion of Assumptions

Several assumptions inherent in the preceding analysis are:

1) The presence of the probe does not disturb the measured density.

The self-collision time for two like particles under Coulomb encounters is given by Spitzer²⁷ as

$$\tau = \frac{11.4 A^{1/2} T^{3/2}}{nZ^4 \ln \Lambda}$$

where $\Lambda = 4.9 \times 10^{14} T^{3/2} / n^{1/2}$ (T in keV). The mean free path is then $\lambda = \bar{v}_{th} \tau$, where $\bar{v}_{th} = (8kT/\pi m)^{1/2}$. Typical values for the cesium arc are given in Table A-I:

TABLE A-I

Summary of Mean Free Path and Momentum Exchange Collision Times for the Plane of the Probe

		Electrons	Ions
$T_i = 0.5$ eV	\bar{v}_{th} cm/sec	6.8×10^7	9.7×10^4
$T_e = 1.0$ eV	τ sec	2.7×10^{-9}	5.6×10^{-7}
$n = 1.5 \times 10^{13}$ cm ⁻³	λ cm	0.18	0.055

Consider a probe in a quiescent plasma. Chen¹² has shown that the collection for a finite-size probe with no applied electric field (probe at plasma potential) is

$$j = \frac{n_{\infty} \bar{v} A_p}{4} \left(\frac{1}{K + \frac{1}{16\pi C D}} \right),$$

where C is the capacitance of the probe, K is a geometric factor, and $D = \lambda \bar{v} / 3$. Therefore, with $A_p = \pi r_p^2$,

$$j = \frac{n_{\infty} \bar{v} A_p}{4} \left(\frac{1}{K + \frac{3A_p}{16\pi \lambda C}} \right).$$

Bohm, Burhop, and Massey²⁸ give a similar expression, with $C \approx 2 (r_p + \lambda) / \pi$, so that

$$j = \frac{n_{\infty} \bar{v} A_p}{4} \left\{ \frac{1}{K + \frac{3\pi r_p^2}{32\lambda(r_p + \lambda)}} \right\}.$$

When $\lambda \gg r_p$, the collection is unaffected by the presence of the probe, and $j = n_{\infty}' \bar{v} A_p/4$, where n_{∞}' is the true plasma density. Hence

$$\frac{n_{\infty}'}{n_{\infty}} = \frac{1}{K + \frac{3\pi r_p^2}{32\lambda(r_p + \lambda)}}.$$

This term represents blockage by the probe body, and r_p is the radius of the entire probe body, not just the collection area.

K varies from 1.0 to 0.5, depending on the relative magnitude of r_p and λ . As $\lambda/r_p \rightarrow \infty$, $K \rightarrow 1$; as $\lambda \rightarrow 0$, $K \rightarrow 1/2$. Thus, K is related to the solid angle subtended by the probe. Thus,

$$K = 1 - \frac{A_{\text{segment}}}{A_{\text{sphere}}},$$

where A_{sphere} is the total solid angle of radius λ and A_{segment} is that portion of the total solid angle that is blocked by the probe. Referring to Fig. A-2, $A_{\text{seg}} = 2\pi\lambda h$, where $h = \lambda(1 - \cos \alpha)$, or $h = \lambda[1 - \cos(\tan^{-1} r_p/\lambda)]$. Then $K = 1 - 1/2 [1 - \cos(\tan^{-1} r_p/\lambda)]$. When $r_p \gg \lambda$, $\tan^{-1} r_p/\lambda \rightarrow \pi/2$, $\cos(\tan^{-1} r_p/\lambda) \rightarrow 0$, and $K \rightarrow 1/2$. When $r_p \ll \lambda$, $\tan^{-1} r_p/\lambda \rightarrow 0$, $\cos(\tan^{-1} r_p/\lambda) \rightarrow 1$ and $K \rightarrow 1$.

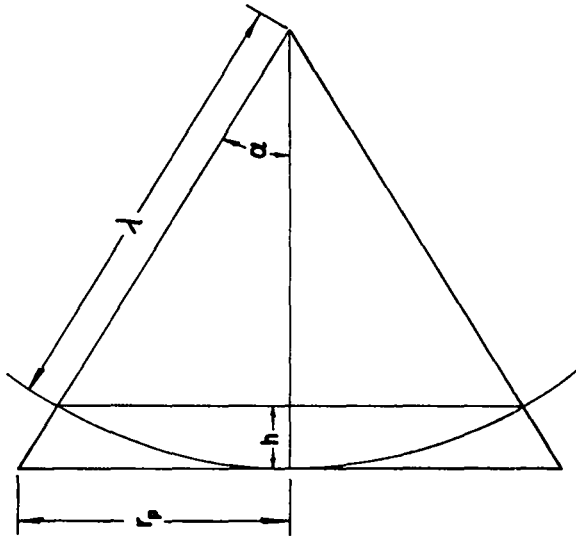


Fig. A-2. Solid angle subtended by probe.

The total diameter of the probe used in the cesium arc is 0.31 cm. For ions, $\lambda_i = 0.055$ cm, $K = 0.663$, and $n_{\infty}'/n_{\infty} = 0.78$. For electrons, $\lambda_e = 0.18$ cm, $K = 0.875$, and $n_{\infty}'/n_{\infty} \approx 1$. The actual density lies between the value derived from electrons and ions, so that the error due to the presence of the probe is probably less than 10%.

Consider now a supersonic plasma stream. The ion current cannot be altered by the presence of the probe; the electron current is undisturbed, as shown in the previous paragraph. Therefore the density measured by a head-on probe in a supersonic plasma stream is the correct density.

2) The magnetic field does not alter the electron current. Sugawara²⁹ has shown that with $T_i/T_e \ll 1$,

$$\frac{j_{e''}}{j_e} = \left[\left(1 + \frac{32\lambda_e}{3\pi r_p} \alpha^{1/2} \right) \right] \left[1 + \frac{32\lambda_e}{3\pi r_p} \alpha^{1/2} \right]^{-1},$$

where $\alpha = [1 + (\omega_e \tau_e)^2]^{-1}$, $j_{e''}$ is the electron current density to the probe in the magnetic field, and j_e is the electron current density in the absence of the magnetic field. The electron-ion mean free path is nearly the same as the electron-electron mean free path, so that $\omega_e \tau_e = 4.8$, for 100 G and the electron values of Table A-I. The radius of the collection area of the probe is now r_p (0.025 cm). These values give $j_{e''}/j_e = 0.88$. Sugawara's theory neglects ambipolar and anomalous diffusion and the effect of finite ion temperature, and therefore overestimates the effect of the magnetic field. All probe measurements were taken at places where the strength of the magnetic field was less than 100 G, so that the effect of the field may be ignored.

3) The plasma is collisionless.

Laframboise³⁰ considers a plasma collisionless for probes if

$$\frac{r_p}{\lambda} \leq \frac{9\pi}{g \ln \left(\frac{12\pi}{g} \right)},$$

where $g = 1/n\lambda_D^3$. λ_D is the Debye length and λ is the mean free path. Numerical values for the cesium arc give $r_p \leq 0.067$ cm for a collisionless regime. This is to be compared with $r_p = 0.025$ cm for the probe used.

Alternatively, the electron mean free path, from Table A-I, is 0.18 cm. The directed velocity of the ions, 2.5×10^5 cm/sec, causes them to travel 0.14 cm between collisions when the mean collision time is 5.6×10^{-7} sec. Both classes of particles travel distances between collisions that are larger than the diameter of the probe collection area.

REFERENCES

1. G. L. Cann, R. A. Moore, P. F. Jacobs, and L. R. Gallagher, "High Specific Impulse Thermal Arc Jet Thrustor Technology," Electro-Optical Systems Inc. Report AFAPL-TR-65, September, 1965.
2. William Grossmann, Jr., Robert V. Hess, and H. A. Hassan, "Experiments with a Coaxial Hall Current Plasma Accelerator," AIAA Journal 3, 1034 (1965).
3. R. R. John, S. Bennett, and J. F. Conners, "Experimental Performance of a High Specific Impulse Arc Jet Engine," Astronautica Acta 11, 97 (1965).
4. P. Brockman, R. Hess, F. Bowen, and O. Jarrett, "Diagnostic Studies in a Hall Accelerator at Low Exhaust Pressure," AIAA Journal 4, 1209 (1966).
5. J. Burlock, P. Brockman, R. V. Hess, and D. R. Brooks, "Measurement of Velocities and Acceleration Mechanism for Coaxial Hall Accelerators," AIAA Journal 5, 558 (1967).
6. A. M. Schneiderman, and R. M. Patrick, "Axial Current Distribution in the Exhaust of the Magnetic Annular Arc," AIAA Journal 5, 249 (1967).
7. A. C. Ducati, G. M. Giannini, and E. Muehlberger, "Experimental Results in High-Specific-Impulse Thermo-Ionic Acceleration," AIAA Journal 2, 1452 (1964).
8. R. M. Patrick and A. M. Schneiderman, "Performance Characteristics of a Magnetic Annular Arc," AIAA Journal 4, 283 (1966).
9. S. Bennett, R. R. John, G. Enos, and A. Tuchman, "Experimental Investigation of the MPD Arc Jet," AIAA Paper 66-239 (1966).
10. K. T. Compton, "On the Theory of the Mercury Arc," Phys. Rev. 37, 1077 (1931).
11. David N. Bowditch, "Investigation of the Discharge and Exhaust Beam of a Small Arc Plasma Thrustor," AIAA Paper 66-195 (1966).
12. F. F. Chen, "Electric Probes," in Plasma Diagnostic Techniques, edited by Richard H. Huddleston and Stanley L. Leonard, Academic Press Inc., New York (1965), Chap. 4.
13. H. M. Mott-Smith and I. Langmuir, "The Theory of Collectors in Gaseous Discharges," Phys. Rev. 28, 727 (1926).
14. H. Driecer, private communication.
15. A. J. Kelly, N. M. Nerheim, and J. A. Gardner, "Electron Density and Temperature Measurements in the Exhaust of an MPD Source," AIAA Journal 4, 291 (1966).
16. Philip Brockman, Robert V. Hess, and Richard Weinstein, "Measurements and Theoretical Interpretation of Hall Currents for Steady Axial Discharges in Radial Magnetic Fields," AIAA Paper 63-382 (1963).
17. Roger P. Henry, "Lorentz Force Maximization in Continuous Flow Hall Current Plasma Accelerators," AIAA Journal 4, 165 (1966).
18. H. Alfvén, "Collision between a Nonionized Gas and a Magnetized Plasma," Rev. Mod. Phys. 32, 710 (1960).
19. D. B. Fradkin, "Modes of Operation of a Lithium Arc Jet," Los Alamos Scientific Laboratory Internal Memorandum.
20. R. A. Moore, G. L. Cann, and L. R. Gallagher, "Performance of Hall Arc Jets with Lithium Propellant," Electro-Optical Systems Inc. Report AFAPL-TR-65-48, Part 1, June 1965.
21. K. Boyer et al., "Theoretical and Experimental Discussion of Ixion, a Possible Thermonuclear Device," Proceedings of the Second United Nations International Conference on the Peaceful Uses of Atomic Energy, Vol. 31, 319 (1958).
22. H. Hügel, G. Kruelle and T. Peters, "Investigations on Plasma Thrusters with Thermal and Self-Magnetic Acceleration," AIAA Journal 5, 551 (1967).
23. Macon C. Ellis, Jr., "Survey of Plasma Accelerator Research," in Proceedings of the NASA-University Conference on the Science and Technology of Space Exploration, Chicago, Illinois, November 1-3, 1962, Vol. 2, pp. 361-81, National Aeronautics and Space Administration Report NASA-SP-11 (1962).
24. R. V. Hess, J. Burlock, J. R. Sevier, and P. Brockman, "Theory and Experiments for the Role of Space Charge in Plasma Acceleration," in Proceedings of the Symposium on Electromagnetics and Fluid Dynamics of Gaseous Plasma, Polytechnic Institute of Brooklyn, April 4-6, 1961, pp. 269-307, Polytechnic Press, New York (1962).
25. D. Bohm, in The Characteristics of Electrical Discharges in Magnetic Fields, Edited by A. Guthrie and R. K. Wakerling, McGraw-Hill Book Company, Inc., New York, (1949), Chap. 3.
26. J. E. Allen, R. L. F. Boyd, and P. Reynolds, "The Collection of Positive Ions by a Probe Immersed in a Plasma," Proc. Phys. Soc. (London) B 70, 297 (1957).
27. Lyman L. Spitzer, Jr., Physics of Fully Ionized Gases, 2nd ed., Interscience Publishers, Inc., New York (1962), p. 133.
28. D. Bohm, E. H. S. Burhop, and H. S. W. Massey, in The Characteristics of Electrical Discharges in Magnetic Fields, Chap. 2.
29. M. Sugawara, "Electron Probe Current in a Magnetized Plasma," Phys. Fluids 9, 797 (1966).
30. J. G. Laframboise, "Theory of Spherical and Cylindrical Langmuir Probes in a Collisionless Plasma at Rest," (June 1966). University of Toronto Institute for Aerospace Studies Report No. 100 (June 1966).